PHYSICAL REVIEW B VOLUME 15, NUMBER 8 15 APRIL 1977

Electronic structure of the F center in CaO†

R. F. Wood
Solid State Division, Oak Ridge National Laboratory, Oak Ridge, Tennessee 37830

T. M. Wilson
Department of Physics, Oklahoma State University, Stillwater, Oklahoma 74074

(Received 3 December 1976)

A theoretical model for calculating the electronic structure of the F center in the alkaline-earth oxides is described; it is a modification of a similar model previously used for the alkali halides. The model emphasizes the importance of (a) electronic structure on the ions neighboring the defect, (b) electronic and ionic polarization of the lattice, and (c) lattice distortion and its effects on the energy levels and wave functions of the defect. Absorption and emission states of the F center in CaO have been calculated using this model. The electron-lattice interaction for A_{1g}, E_g, and T_{2g} displacements of the nearest-neighbor ions has been calculated and used to interpret the absorption and luminescence bands of the F center. The calculated energy-level scheme as a function of lattice relaxation gives substantial agreement with published experimental data. It indicates that the $^1T_{1u} \rightarrow {}^1A_{1g}$ and $^3T_{1u} \rightarrow {}^1A_{1g}$ transitions should occur at roughly 2.0 eV and give rise to two emission bands with different temperature dependence. The $^3T_{1u}$ relaxed excited state is predominantly coupled to the E_g vibrational modes. Unlike the other states its wave function is a rapidly varying function of A_{1g} lattice distortion. The calculations suggest that an absorption band associated with the $^3T_{1u} \rightarrow {}^3A_{1g}$ transition may be observable at roughly 0.7 eV using techniques for excited-state spectroscopy.

I. INTRODUCTION

In this paper we describe calculations of the electronic structure of the F center (two electrons trapped at an O^{2-} vacancy) in CaO.[1] These calculations are based on methods previously developed for point defects in alkali halides, e.g., the F center,[2-4] U center,[5,6] M center,[7] and excitons.[8] During the past few years we have been extending and modifying these methods for applications to defects in the alkaline-earth oxides. Our work to date includes calculations on both the one- (F^+) and two-electron centers in MgO, CaO, and SrO. It has become apparent during the course of this work that the two centers in these oxides must be treated differently and that in many ways the two electron center is in fact the simplier of the two. To keep this paper at a reasonable length, we will restrict the discussion to certain aspects of the absorption and emission of the two electron center in CaO.

The model on which the calculations of Refs. 2–8 and those to be described here have been based emphasizes the importance of (a) the electronic structure of the ions neighboring the defect, (b) the electronic and ionic polarization of the lattice, and (c) lattice distortion. The structure of the neighboring ions gives rise to coulomb, exchange and overlap repulsive contributions to the energy. Although these contributions often may be relatively small compared to the Madelung energy they change significantly from state to state and must be included. The electronic and ionic polarization effects are also important for the energy and are frequently crucial for the determination of the wave functions. Because of the polarization effects, small changes in energy may be accompanied by large changes in the spatial extent of the wave functions. The inclusion of lattice distortion or relaxation is essential for determining the Stokes shift between absorption and emission and for calculating the electron-phonon coupling at the defect site. Our computer programs enable us to calculate this coupling for A_{1g}, E_g, and T_{2g} modes of lattice distortion. In other work, which we hope to complete shortly, the results of the present calculations will be used to describe the shapes of the absorption and emission bands including the vibronic structure which is observed in the emission spectrum from the triplet state of the F center in CaO.

The model described here is not an entirely "first principles" one since it contains certain parameters of the perfect crystal which may be taken as adjustable when not known. The basic model worked rather well for the alkali halides with relatively little adjustment of parameter values taken from the literature, but we found a different situation in the alkaline-earth oxides. We attribute this in large measure to two factors. The first of these simply reflects the cruder state of knowledge (relative to the alkali halides) of

many important parameters in the oxides. We have in mind such quantities as the electron affinity of the crystal, the effective mass at the bottom of the conduction band, the repulsive parameters in Born-Mayer potentials, van der Waals interaction parameters, etc. The second factor stems from the doubly charged character of the ions in the oxides; this affects the calculations in two major ways. First, the energy levels and wave functions are more sensitive to the positions of the neighboring ions than is the case in the alkali halides. Second, the electronic structure of the O^{--} ion is more complex than that of the negative halide ions. The O^{--} ion, although unstable in free space, is stabilized and made fairly compact in the crystal by the action of the Madelung potential; its orbitals are therefore strongly crystal dependent. We expect most ion-ion overlap intergrals to be significantly larger in the oxides than in the halides and our calculations indicate that this is indeed the case. We also expect it to be difficult to adequately treat the polarizability of the O^{--} ion because it may depend strongly on its crystal environment, e.g., the charge at the defect site. We believe that our parametrization of the calculations can be made more plausible and reliable by the requirement that the values of the parameters be essentially the same in both the F and F^+ center calculations. Also the present calculations have benefitted greatly from the experimental data that has accumulated in recent years, some of which we will summarize in Sec. II. In Sec. III, the model used in the present calculations is outlined and in Sec. IV the details and results of these calculations are given. In Sec. V the theoretical and experimental results are compared and discussed in relationship to the model.

II. REVIEW OF PREVIOUS WORK

Many experimental papers have appeared in recent years on the optical and magnetic properties of point defects and color centers in the alkaline-earth oxides. Two useful reviews[9,10] of the literature have appeared fairly recently; here we will outline only the most current information on the optical properties of the F center in CaO.

F-center absorption bands have been identified in the spectra of MgO, CaO, SrO, and BaO, but the corresponding emission spectra have been positively identified only for MgO and CaO. The absorption band of the F center arises from an allowed transition from the $^1A_{1g}$ ground state to one or more $^1T_{1u}$ excited states. Since the ground state of the F center is diamagnetic, it has no EPR signal and consequently must be detected optically. Both the F^+ and F centers in MgO have absorption bands at about 5 eV and there was initially some uncertainty about the correctness of their identification.[11] Unlike the situation in MgO, the F^+ and F center absorption bands are well separated in CaO with peaks at 3.7 and 3.1 eV, respectively.[12] The emission spectrum obtained by exciting in the 3.1-eV band in CaO has been studied by Henderson *et al.*[13] They associated two bands, one at 2.5 eV and the other at 2.0 eV, with the F center. From the lifetime studies of these transitions they concluded that the 2.0-eV band corresponds to the $^3T_{1u} \rightarrow {}^1A_{1g}$ transition, and that the 2.5-eV band corresponds to the $^1T_{1u} \rightarrow {}^1A_{1g}$ transition. However, a recent study of the luminescence spectrum by Bates and Wood,[14] stimulated by the theoretical calculations reported herein and in Ref. 1, shows no trace of the 2.5-eV band; they suggest that it may have originated from transition-metal impurities which are difficult to remove from CaO. The temperature dependence of the 2.01-eV band shows a continuous shift of intensity into a high-energy shoulder at 2.05 eV as the temperature is raised above 300 °K.[15] At the same time, the lifetime of the luminescence decreases rapidly indicating that this shoulder is probably associated with the $^1T_{1u} \rightarrow {}^1A_{1g}$ emission. Studies of the paramagnetic resonance of the emitting level involved in this emission line at low temperatures clearly showed that it has a substantial spin-triplet component.[16] These measurements further indicated a strong Jahn-Teller coupling to the E_g vibrational modes, and from later work on the stress splittings of the zero-phonon line,[17] it was concluded that the coupling to A_{1g} and T_{2g} modes is weak.

Unlike the situation in the alkali halides, there have been relatively few theoretical calculations made on the F center in the alkaline-earth oxides. Neeley and Kemp[18] have reported the results of a linear-combination-of atomic-orbitals calculation using Gaussian-type orbitals for the F center in MgO and CaO. This calculation was made using the point-ion lattice model, without taking into account lattice relaxation and polarization corrections. Their prediction for the $^1A_{1g} \rightarrow {}^1T_{1u}$ absorption energy was 4.4 eV in CaO. Bennett[19] has reported a more extensive calculation of the F center in MgO and CaO. His model involved the numerical solution of the Hartree-Fock-Slater equations[20] to obtain the orbitals for the defect electrons centered on an anion vacancy, again using a point-ion lattice potential. The effects of ionic polarization of the nearest-neighbor ions and estimates for the correlation energy of the defect electrons were included. Bennett found the absorption energies to be 3.9 eV in MgO and

3.15 eV in CaO. These calculations also predicted energies for the $^3T_{1u} \rightarrow {}^1A_{1g}$ emission peak of 2.53 eV in MgO and 1.93 eV in CaO, and 3.10 eV for the $^1T_{1u} \rightarrow {}^1A_{1g}$ emission peak in CaO.

III. THEORETICAL MODEL

In this section we describe our model for calculations of the electronic structure of the F center in the alkaline-earth oxides. This model is based in large part on developments in earlier papers,[3,6] to which we frequently refer in order to avoid excessive duplication.

A. Effective Hamiltonian and wave functions

Following the development in Ref. 6 for the U center in alkali halides, the spin-independent electronic Hamiltonian for a single two-electron F center in an otherwise perfect crystal with $M-2$ electrons is written in atomic units as

$$\overline{\mathcal{H}}(1,2,\ldots,M) = \mathcal{H}(1,2) + \mathcal{H}_{cr}(3,\ldots,M) + \mathcal{H}_{int}(1,2,\ldots,M), \quad (1)$$

where

$$\mathcal{H}(1,2) = -\tfrac{1}{2}\nabla_1^2 - \tfrac{1}{2}\nabla_2^2 + r_{12}^{-1}, \quad (2)$$

$$\mathcal{H}_{cr}(3,\ldots,M) = \sum_{l=3}^{M}\left(-\tfrac{1}{2}\nabla_l^2 - \sum_{\nu\neq 0}\frac{Z_\nu}{|\vec{r}_l - \vec{R}_\nu|} + \sum_{k>l}^{M} r_{kl}^{-1}\right), \quad (3)$$

and

$$\mathcal{H}_{int}(1,2,\ldots,M) = \sum_{i=1}^{2}\left(-\sum_{\nu\neq 0}\frac{Z_\nu}{|\vec{r}_i - \vec{R}_\nu|} + \sum_{l=3}^{M} r_{il}^{-1}\right). \quad (4)$$

Here Z_ν is the atomic number of the ion at position $\vec{R}_\nu$, $\vec{r}_l$ is the spatial coordinate of the lth electron and r_{il}^{-1} is the mutual electronic interaction. The electronic wave function is

$$\Psi(1,2,\ldots,M) = [M!/2!(M-2)!]^{1/2}\mathcal{A}\psi(1,2)\times\Phi(3,4,\ldots,M). \quad (5)$$

Here, ψ is the two-electron group function for the F electrons, Φ is an $(M-2)$-electron function for the rest of the crystal, and $\mathcal{A}$ is the antisymmetrizing operator. The ith numerical argument denotes both the space and spin coordinates of the ith electron. If we assume that ψ and Φ are separately antisymmetrized it can be shown that

$$\mathcal{A} = [M!/2!(M-2)!]^{-1}\sum_P (-1)^p P(d,c). \quad (6)$$

The permutation operator P exchanges electrons between the defect group d and the crystal group c but not within the two groups; p is the parity of the permutation. We assume that strong orthogonality holds, i.e.,

$$\int \psi(1,2)\Phi(3,4,\ldots,k-1,1,k+1,\ldots,M)\,d\tau_1 = 0, \quad (7)$$

and that ψ and Φ are separately normalized. This type of wave function will allow for correlation effects within the two groups, but excludes intergroup correlations except those introduced by the antisymmetrization. These intergroup effects will be taken into account approximately through the polarization terms to be added in Sec. III B.

The orthogonality condition of Eq. (7) makes it possible to write the expectation value of $\overline{\mathcal{H}}$ [Eqs. (1)–(4)] with respect to Ψ of Eq. (5) as

$$\langle\Psi|\overline{\mathcal{H}}|\Psi\rangle = \langle\psi|\mathcal{H}|\psi\rangle + [M!/(M-2)!2!]\times\langle\psi\Phi|\mathcal{H}_{int}\mathcal{A}|\psi\Phi\rangle + \langle\Phi|\mathcal{H}_{cr}|\Phi\rangle. \quad (8)$$

In obtaining this expression, we have used the property of $\overline{\mathcal{H}}$ that it is symmetric in the electron coordinates and therefore commutes with the antisymmetrizer $\mathcal{A}$, and the property of $\mathcal{A}$ that it is a projection operator ($\mathcal{A}^2 = \mathcal{A}$). As in earlier work (Refs. 3–6), the third term in Eq. (8) will be treated within the framework of classical ionic crystal theory. The first and second terms in Eq. (8) will be expressed in the form of an expectation value of an effective two-electron Hamiltonian derived below.

We approximate the two-electron function on the right-hand side of Eq. (5) by the expansion

$$\psi^{\pm}(1,2) = \sum_{k=1}^{n} C_k\psi_k^{\pm}(\vec{r}_1,\vec{r}_2)\chi_{\mp}(\xi_1,\xi_2), \quad (9)$$

in which "+" implies a singlet state of the F center and "−" implies a triplet. The spin function $\chi_{\mp}(\xi_1,\xi_2)$ is given by

$$\chi_{\mp}(\xi_1,\xi_2) = [\alpha(\xi_1)\beta(\xi_2) \mp \alpha(\xi_2)\beta(\xi_1)]/\sqrt{2}. \quad (10a)$$

The two-electron basis function

$$\psi_k^{\pm}(\vec{r}_1,\vec{r}_2) = N_k[f_{k1}(\vec{r}_1)f_{k2}(\vec{r}_2) \pm f_{k2}(\vec{r}_1)f_{k1}(\vec{r}_2)], \quad (10b)$$

where N_k is a normalization factor. The notation emphasizes that in order to determine the kth two-electron function it is necessary to specify two, i.e., $k1$ and $k2$, orbitals. This type of function allows for radial but no angular correlation of the F-center electrons. In heliumlike ions a few terms of the form of Eq. (10b) can introduce approximately 85% of the total correlation energy.

We imagine Φ to be approximated by a single Slater determinant in which each one-electron

orbital is thought of as a Wannier function localized about one of the ions in the crystal. As in Refs. 3–6, we assume the Wannier functions can be replaced, to a good enough approximation, by free-ion self-consistent-field (SCF) wave functions or by the crystal-adapted SCF localized orbitals introduced and used extensively by Kunz[21] and coworkers. If we let $\phi_j(\vec{r}-\vec{R}_\nu) \equiv \phi_{\nu j}(\vec{r})$ be the jth one-electron orbital on the νth ion then the orthogonality of $\psi_k(\vec{r}_1, \vec{r}_2)$ to Φ is assured by requiring the functions f_{ki} to be orthogonal to the functions $\phi_{\nu j}$. The latter condition is satisfied by writing

$$f_{ki}(\vec{r}) = \bar{N}_{ki}\left(f^0_{ki}(\vec{r}) - \sum_{\nu j} \phi_{\nu j}(\vec{r})\langle\phi_{\nu j}|f^0_{ki}\rangle\right) . \quad (11)$$

where $\bar{N}_{ki}$ is another normalization factor, and the f^0_{ki} are of the form

$$f^0(\vec{r}) = [(2\beta^{2n+1}/(2n)!]^{1/2} r^{n-1} e^{-\beta r} \mathcal{K}_{\Gamma p}(\theta, \phi) . \quad (12)$$

$\mathcal{K}_{\Gamma p}$ is the cubic harmonic for the pth component of the irreducible representation Γ of the O_h point group. The integer n in $f^0(r)$ is fixed once a reasonably optimal choice is determined by trial and error, but β is a true nonlinear variational parameter. Thus even a few terms in the expansion of Eq. (9) give a quite flexible trial function.

Under the assumptions of our model as developed thus far, the first and second terms of Eq. (8) can be expressed in terms of an effective two-electron Hamiltonian which acts only on $\psi(1, 2)$. Thus,

$$H(1, 2) = \sum_{i=1}^{2} h_1(\vec{r}_i) + r_{12}^{-1} , \quad (13)$$

with

$$h_1(\vec{r}) = -\tfrac{1}{2}\nabla^2 - \sum_\nu \{(Z_\nu - N_\nu)|\vec{r}-\vec{R}_\nu|^{-1} + U_\nu(r)\} , \quad (14)$$

where N_ν is the number of electrons on the νth ion. The effective potential U_ν originates entirely from the second term of Eq. (8). It is generated from the relevant localized SCF orbitals contained in $\Phi(3\cdots M)$ and the nuclear charge on the νth ion. In our approach, the original nonlocal Hartree-Fock exchange is replaced by an equivalent set of local exchange potentials which are weakly energy dependent and strongly l dependent. To be consistent with this replacement, a set of one-electron orbitals slightly modified from the original free-ion set must be introduced at appropriate points, e.g., for the $\phi_{\nu j}$ in Eq. (11). The generation of these effective potentials and orbitals is described in detail in Refs. 3 and 4. Note that the first two terms in the above expression for h_1 give just the point-ion model, while the third term gives the effects of the electronic structure on the neighboring ions, e.g., Coulomb penetration and exchange energies.

In the potentials which describe the Coulomb and exchange interactions between the defect electrons and all of the other $M-2$ electrons in the crystal, it is desirable to truncate the sum over ν. This leads us to define a radius R_0 within which we treat explicitly all of the interactions of the F-center electrons with their neighbors by Eq. (13), and outside of which we approximate h_1 by the effective-mass expression

$$h_1(\vec{r}) = -(1/2m^*)\nabla^2 + \epsilon_{HF} - 2/r , \quad r > R_0 . \quad (15)$$

Here m^* is the effective mass and ϵ_{HF} is the energy of the bottom of the conduction band in the Hartree-Fock approximation (we assume a simple band structure in which the minimum of the conduction band occurs at the Γ point). The potential of an O^{2-} vacancy is approximated in the outer region by $-2/r$ in the alkaline-earth oxides.

In the present work, we have chosen R_0 to lie in the range $a_0 < R_0 < \sqrt{2}\, a_0$, where a_0 is the first-nearest-neighbor (1nn) distance. Hence, we have taken the electronic structure of only the 1nn ions explicitly into account in the calculations discussed in this paper. The structure on more-distant ions is included implicitly in the effective-mass approximation and through the dielectric polarization which we now introduce. The reason for this choice will be discussed further in Sec. V.

B. Inclusion of dielectric polarization

When either one of the F-center electrons moves out of the vacancy, local polarization of the crystal is set up. It has been stressed in the earlier calculations of F and U centers in the alkali halides that dielectric polarization effects must be included in defect calculations to obtain satisfactory agreement with experiment. This is not surprising because the excited states of many color centers are effective-mass-like and lie close to the bottom of the conduction band.

As in earlier papers,[3-6] we have included the principal polarization effects in our calculations by adding potentials of the type introduced by Toyozawa[22] and Haken and Schottky[23] (THS) for the electronic polaron to the Hamiltonian of Sec. III A. The polarization potential of each electron and its corresponding hole can be broken into two parts, i.e.,

$$U_p(r) = U_{el}(r) + U_{ion}(r) . \quad (16)$$

U_{el} gives the contribution due to the distortion of the electronic orbitals on the neighboring ions (electronic polaron), and U_{ion} gives the contribution due to the displacements of the ions (ionic polaron). The forms of these potentials are

$$U_{el}(r) = -\tfrac{1}{2}(1-\kappa_\infty^{-1}) \{(\rho_e+\rho_h) - (1/r)[2-\exp(-\rho_e r) - \exp(-\rho_h r)]\} \quad (17a)$$

and

$$U_{ion}(r) = -\tfrac{1}{2}(\kappa_\infty^{-1}-\kappa_{st}^{-1}) \{(v_e+v_h) - (1/r)[2-\exp(-v_e r) - \exp(-v_h r)]\}. \quad (17b)$$

κ_∞ and κ_{st} are the high-frequency and static dielectric constants, respectively. The constants ρ_e, ρ_h, v_e, and v_h are discussed in some detail in Refs. 3 and 4. The significance of ρ_e and ρ_h is easy to understand by considering the following limit:

$$-\frac{1}{r}+U_{el}(r) \xrightarrow[r\to\infty]{} -\frac{1}{\kappa_\infty r} - \tfrac{1}{2}(1-\kappa_\infty^{-1})(\rho_e+\rho_h). \quad (18a)$$

From classical electrostatics, the polarization energy to remove a unit electronic charge from a cavity of radius R in a dielectric medium is $-\frac{1}{2}(1-\kappa^{-1})/R$. The value of κ to be used will depend on whether one assumes only the electronic polarization or both the electronic and ionic polarization can follow the removal of the charge. Here we have made the former assumption and find that our expressions reduce to the correct form if ρ_e and ρ_h are appropriately chosen reciprocal radii. We chose them by taking $\rho_e=\rho_h=\rho$ and determining ρ_h from the equation

$$U_{ML}^- = \tfrac{1}{2}(1-\kappa_\infty^{-1})\rho_h. \quad (18b)$$

U_{ML}^- gives the electronic polarization energy associated with the removal of a unit negative charge from the crystal in a Mott-Littleton-type[24] calculation in which lattice relaxation is not allowed. This type of calculation will be discussed briefly below. We could have used a similar equation for determining ρ_e from U_{ML}^+ but this would be equivalent to assuming that an electron transferred out of the vacancy remains tightly bound to some positive ion in the crystal and this cannot be correct. In absence of more-detailed information about this point and in view of other approximations in the model we feel justified in putting $\rho_e=\rho_h$.

Let us now consider the following limit:

$$-\frac{1}{r}+U_{el}(r)+U_{ion}(r) \xrightarrow[r\to\infty]{} -\frac{1}{\kappa_{st} r} - (1-\kappa_\infty^{-1})\rho - \tfrac{1}{2}(\kappa_\infty^{-1}-\kappa_{st}^{-1})(v_e+v_h). \quad (19a)$$

Here we have assumed that the ions as well as the electrons can follow the motion of the electrons and holes involved. This is reflected in the screening of the $1/r$ potential by the full static dielectric constant κ_{st} and in the additional term in v_e and v_h which can be thought of as the self-energy of polarization due to ionic displacements. The THS theory of Wannier excitons suggests the prescription

$$v_e = (2m_e^* \omega_{LO}/\hbar)^{1/2}, \quad (19b)$$

where ω_{LO} is the longitudinal-optical phonon frequency. We have used this equation as a guide in choosing both v_e and v_h but the justification for it is hardly reliable, and we have felt free to vary both v_e and v_h over fairly wide ranges. Further discussions of some of the problems associated with the THS form are given in Refs. 3 and 4.

Our concern with these polarization terms should become more obvious when one considers that an optical transition from a state in which the electron is in the vacancy to a hydrogenic effective-mass state occurs in the order of 10^{-16} sec. A typcial lattice relaxation time however is of the order of 10^{-12} sec. Since both F-center electrons are well confined to the vacancy in the ground state of CaO, the screening of the vacancy by the electrons in this state is nearly complete beyond the 1nn ions. Thus we have set $v_e=v_h=0$ in absorption (but not in emission) so that $U_{ion}=0$. Contributions from the static displacement of the 1nn ions will still be allowed through the calculation of the lattice relaxation energy using classical ionic crystal theory.

Because the F center in the alkaline-earth oxides has two defect electrons, additional electronic polarization terms appear which were not encountered in the earlier one-electron F-center calculations[3,4] of the alkali halides. When one of the two F electrons is excited out of the vacancy, it sets up an electronic polarization field that acts back on the defect electron still within the vacancy. This is a repulsive interaction and raises the energy of the remaining electron. However, this field also acts back upon two holes which we can loosely think of as representing the doubly charged vacancy; these holes remain well localized in the vacancy and their energies are lowered by the induced polarization potential. The sum of these contributions reduces to that resulting from the THS terms, as long as one electron remains in the vacancy region to exactly cancel one of the hole contributions. For the limiting case in which both electrons are removed from the vacancy region, it becomes necessary to subtract from the THS contributions an additional energy $(1-\kappa_\infty^{-1})\rho_h$. This term arises from the fact that when both electrons are removed from the defect region, the vacancy

has a single effective charge of +2 and the THS terms treat the problem as though there were two singly charged holes present. We include this contribution to the energy through the approximation

$$U_p^{12}(R_0) = -(1-\kappa_\infty^{-1})\rho_h[\Theta(r_1-R_0)\Theta(r_2-R_0)]. \tag{20}$$

The Heaviside step function is defined by $\Theta(x)=0$, $x<0$; $\Theta(x)=1$, $x>0$. This term makes only a small contribution to the ground-state energy in CaO because both electrons are well localized within the vacancy region, and to the first-excited states because, although one of the defect electrons has been excited out of the vacancy region, the second remains well localized. In fact, the choice of the radius R_0 is not very critical.

We are now in a position to write the final form for our total effective two-electron Hamiltonian, including the effects of dielectric polarization but neglecting lattice relaxation. We rewrite Eq. (13) as

$$H(1,2) = \sum_{i=1}^{2} h_1(r_i) + g_{12}, \tag{21a}$$

with

$$h_1(\vec{r}) = -\tfrac{1}{2}\nabla^2 - \sum_\nu \{(Z_\nu - N_\nu)\,|\,\vec{r}-\vec{R}_\nu\,|^{-1} + U_\nu(\vec{r})\} + U_p(r), \quad r<R_0, \tag{21b}$$

$$h_1(\vec{r}) = -\frac{1}{2m^*}\nabla^2 + \epsilon_{\mathrm{HI}} - \frac{2}{r} + U_p(r), \quad r>R_0, \tag{21c}$$

and for all values of $\vec{r}_1$ and $\vec{r}_2$,

$$g_{12}(\vec{r}_1,\vec{r}_2) = r_{12}^{-1} + U_p^{12}(R_0). \tag{21d}$$

It should be pointed out here that the THS forms for the polarization potentials in Eqs. (17a) and (17b) do not depend directly on the positions of the neighboring ions. This is unfortunate because as the six 1nn ions begin to relax, the dipoles induced by the effective charge of the defect will change as will their mutual interaction energy. Since the charge of the defect depends on wavefunctions which change with the state of excitation and with the position of the neighboring ions, the polarization energy and its change from state to state are a function of lattice relaxation. These effects are small but important in determining both the extent of relaxation and the excitation energies; they will be approximated below.

C. Lattice relaxation

To complete the description of a model which is sufficiently detailed to cope with most of the available experimental data, we must now consider how to include the contributions of lattice relaxation to the total energy of the crystal containing the defect. These effects arise explicitly through the ion-core orthogonalization terms in the orbitals of Eq. (11) and from the second and third terms on the right-hand side of Eq. (8). Relaxation effects from the second term are mostly included in the effective one-electron Hamiltonians of Eqs. (14) and (21b). Both $U_\nu(\vec{r}) \equiv U(\vec{r}-\vec{R})$, which contains two-electron Coulomb and exchange potentials, and the point-ion potential are explicitly dependent on the position of the neighboring ions. Small contributions also come from the above-mentioned change in the polarization potentials of Eqs. (17a) and (17b) as the ions move. Lattice-relaxation effects due to the third term would be exceedingly difficult to treat purely quantum mechanically. Such a calculation appears both premature and unnecessary at this point since it would not likely yield great accuracy and would be expensive in computer time. This is why we have treated the term $E_{\mathrm{cr}} \equiv \langle \Phi \,|\, \mathcal{H}_{\mathrm{cr}} \,|\, \Phi \rangle$ in Eq. (8) using variations of the well-known Mott-Littleton procedure for defect calculations.

Let us define symmetrized displacements of the equivalent ions in a shell n about a defect or impurity. These are linear combinations of individual ionic displacements which transform according to the irreducible representations of the point group; they can be expressed by

$$Q_n(\Gamma p) = u \sum_j \vec{e}_{nj}(\Gamma p). \tag{22}$$

Here, as in Eq. (12), Γ and p label the irreducible representations and their components, respectively; j runs over the ions in the nth shell. The vectors $\vec{e}_{nj}(\Gamma p)$ can be chosen such that

$$Q_n(\Gamma p)\cdot Q_n(\Gamma' p') \equiv u^2 \sum_j \vec{e}_{nj}(\Gamma p)\cdot \vec{e}_{nj}(\Gamma' p') = u^2 \delta_{\Gamma\Gamma'}\delta_{pp'}. \tag{23}$$

Table I gives the vectors $\vec{e}_{nj}(\Gamma p)$ for the even modes of the (100) shell. For clarity and simplicity we assume that only the 1nn ions displace according to the various symmetry modes of O_h. This does not mean that we neglect the displacement of more distant ions but these are assumed to undergo only A_{1g}-type distortions. Furthermore, their displacements are generally, but not always, calculated from dielectric continuum theory. In this manner the so-called configuration-coordinate (CC) curves to be constructed below can be conveniently related to a single-relaxation parameter for that mode. It can be shown, and indeed it is widely known, that for octahedral

symmetry only the A_{1g}, E_g, and T_{2g} modes of the 1nn ions alter the transition energy between A_{1g} and T_{1u} electronic states; Therefore these are the only vibrational modes of interest to us.

It would be impractical to describe here in detail the model and the computer program on which the lattice-relaxation calculations are based. Major portions of it are discussed in a paper by Mostoller and Wood.[25] The entire calculation follows closely the work of Boswarva and Lidiard[26] in which the Mott-Littleton model was refined and applied to Frenkel defect calculations in the alkali halides. We can sketch this type of calculation as follows. The total change in E_{cr} is expressed as

$$\Delta E_{cr}(\delta) = \Delta E_C(\delta) + \Delta E_r(\delta) + \Delta E_p(\delta) \quad (24)$$

in which the subscripts C, r, and p stand for coulomb, repulsive, and polarization, respectively. The relaxation or distortion parameter δ gives the displacement of the 1nn ions as a percentage of the nearest-neighbor distance in the perfect crystal. In the Mott-Littleton approach the crystal is divided into an inner region (region I) immediately surrounding and including the defect and an outer region (region II) made up of the remainder of the crystal. In region I, the ions are treated electrostatically as point charges and point dipoles and the repulsive interactions are approximated by combined Born-Mayer and van der Waal potentials. In region II, the crystal is treated as a polarizable continuum in which the electronic and displacement dipole moments per unit volume induced by the effective charge of the defect act back on the point monopoles and dipoles in region I. The change in this interaction energy is not included in the THS formulation and must be calculated here. It becomes important only for rather diffuse states. The calculation of the electrostatic and repulsive interaction is straightforward. In fact, $\Delta E_C(\delta)$ and $\Delta E_r(\delta)$ have been taken from Eqs. (22) and (23) of Ref. 3 with suitable modification for the doubly charged ions in CaO and with the inclusion of van der Waals forces (see Boswarva and Lidiard[26]).

TABLE I. Vector ionic displacements $\vec{e}_j(\Gamma_p) = N\vec{\sigma}_j(\Gamma_p)$ for the even modes of (100) shells in cubic crystals. The N's are normalization constants, $j = 1$–6 labels the ions at (100), (010), (001), ($\bar{1}$00), (0$\bar{1}$0), (00$\bar{1}$), respectively, and $\hat{x}, \hat{y}, \hat{z}$ denote unit vectors along the Cartesian axes.

Γ_P	N	$\vec{\sigma}_1$	$\vec{\sigma}_2$	$\vec{\sigma}_3$	$\vec{\sigma}_4$	$\vec{\sigma}_5$	$\vec{\sigma}_6$
A_{1g}	$1/\sqrt{6}$	$\hat{x}$	$\hat{y}$	$\hat{z}$	$-\hat{x}$	$-\hat{y}$	$-\hat{z}$
$E_g\epsilon$	$1/2\sqrt{3}$	$-\hat{x}$	$-\hat{y}$	$2\hat{z}$	$\hat{x}$	$\hat{y}$	$-2\hat{z}$
E_gG	$\frac{1}{2}$	$\hat{x}$	$-\hat{y}$	0	$-\hat{x}$	$\hat{y}$	0
$T_{2g}x$	$\frac{1}{2}$	0	$\hat{z}$	$\hat{y}$	0	$-\hat{z}$	$-\hat{y}$
$T_{2g}y$	$\frac{1}{2}$	$\hat{z}$	0	$\hat{x}$	$-\hat{z}$	0	$-\hat{x}$
$T_{2g}z$	$\frac{1}{2}$	$\hat{y}$	$\hat{x}$	0	$-\hat{y}$	$-\hat{x}$	0
$T_{1g}x$	$\frac{1}{2}$	0	$\hat{z}$	$-\hat{y}$	0	$-\hat{z}$	$\hat{y}$
$T_{1g}y$	$\frac{1}{2}$	$-\hat{z}$	0	$\hat{x}$	$\hat{z}$	0	$-\hat{x}$
$T_{1g}z$	$\frac{1}{2}$	y	$-\hat{x}$	0	$-\hat{y}$	$\hat{x}$	0

The induced-polarization terms offer more difficulty but again they can be extracted from the work of Boswarva and Lidiard. Here, however, we write them in the form

$$\Delta E_p(\delta) = \Delta E_{p1}(\delta) + \Delta E_{p2}(\delta) \ , \quad (25)$$

with

$$\Delta E_{p1}(\delta) = -\frac{3}{a_0}\left(\frac{\beta_+(1+\delta)^3}{2.371\beta_+ + (1+\delta)^3}\right) \times D(\delta)(D(\delta) - q_{2nn}M) \ , \quad (26)$$

$$D(\delta) \equiv \left(\frac{q_{1nn} + \sqrt{2}\,Q + 0.25Q}{(1+\delta)^2} - \frac{4Q(1+\delta)}{(2+2\delta+\delta^2)^{3/2}} - \frac{Q}{(2+\delta)^2}\right) \ ,$$

$$M \equiv \frac{1}{2\pi}\,\frac{(1-\kappa_\infty^{-1})(0.388\alpha_+ + 1.965\alpha_-)}{\alpha_+ + \alpha_-} \ ,$$

and

$$\Delta E_{p2}(\delta) = (3/a_0)Qq_{2nn}M\delta \ . \quad (27)$$

In these equations $\beta_+ \equiv \alpha_+/a_0^3$; q_{1nn} and q_{2nn} are the effective charges of the defect within the first- and second-nearest-neighbor shells, respectively; α_+ and α_- are the polarizabilities of the positive and negative ions; and $Q = 2$ for the alkaline-earth oxides. Equation (26) gives the energy of interaction of the effective charge at the vacancy with the dipoles on the 1nn ions plus the change in the energy of the 1nn ions in the field of the induced dipoles on the other five 1nn ions. Equation (27) gives the energy due to the displacement of the 1nn ions in the induced dipole field of the region II ions (2nn's and beyond). The charges q_{1nn} and q_{2nn} were evaluated using the wavefunctions obtained from the calculation of the electronic energy described in Secs. III A and III B. Although fairly small, these polarization terms were included directly in the minimization procedure and not treated as perturbations.

D. Matrix elements of the secular equation

From the contents of Secs. III A–III C we are able to write an expression for the change in the total energy of the system as a function of the positions of the ions in the crystal. Portions of this calculation involve the solution of the secular equa-

tion

$$\det(H - ES) = 0 \tag{28}$$

derived from the usual variational problem. In our present case, the matrix elements of this secular equation will be given in terms of an effective two-electron Hamiltonian which, in an approximate way, takes into account the many-body effects due to all of the other electrons and nuclei in the crystal. This Hamiltonian is defined by Eqs. (2a)–(2d) and the trial wave function by Eq. (9); the matrix elements of $H(1,2)$ are taken with respect to the two electron function given in Eq. (10b).

The matrix elements of the overlap matrix S in Eq. (28) are given by

$$S_{kl}^{\pm} = N_k N_l [S_{k_1,l_1} S_{k_2,l_2} \pm S_{k_1,l_2} S_{k_2,l_1}] \ , \tag{29}$$

with

$$S_{ki,lj} = \bar{N}_{ki} \bar{N}_{lj} \left(S^0_{ki,lj} - \sum_{\mu,m} \langle f^0_{ki} | \phi_{\mu m} \rangle \langle \phi_{\mu m} | f^0_{lj} \rangle \right) \tag{30}$$

and

$$\bar{N}_{ki} = \left(1 - \sum_{\mu,m} |\langle f^0_{ki} | \phi_{\mu m} \rangle|^2 \right)^{-1/2} \ .$$

We have assumed that the $\phi_{\mu m}$ on different 1nn sites do not overlap.

The matrix elements of the one-electron part of the Hamiltonian $H(1,2)$ are given by

$$h_{kl}^{\pm} = N_k N_l \{ S_{k_1,l_1} h_{k_2,l_2} + S_{k_2,l_2} h_{k_1,l_1} \pm [S_{k_1,l_2} h_{k_2,l_1} + S_{k_2,l_1} h_{k_1,l_2}] \} \ . \tag{31}$$

The matrix elements of the one-electron operator $h_{ki,lj}$ were derived in an earlier paper[3] in the same approximation used here.

The two-electron matrix elements of the effective Hamiltonian are given by

$$\langle \psi_k^{\pm} | g_{12} | \psi_l^{\pm} \rangle = N_k N_l [\langle f_{k_1} f_{k_2} | g_{12} | f_{l_1} f_{l_2} \rangle \pm \langle f_{k_1} f_{k_2} | g_{12} | f_{l_2} f_{l_1} \rangle] \ . \tag{32}$$

For the Coulomb interaction r_{12}^{-1}, these integrals were evaluated through second order in overlap using the approximation[27]

$$f^0_{ki} \phi_{\mu m} \approx \langle f^0_{ki} | \phi_{\mu m} \rangle | \phi_{\mu m} |^2 \ .$$

The matrix elements involving the polarization potential given by Eq. (20) are very small and will not be discussed further here.

IV. DETAILS AND RESULTS OF THE CALCULATIONS

A. A_{1g} configuration-coordinate curves—Absorption

We have constructed configuration-coordinate (CC) curves which give the behavior of the various electronic states in absorption as a function of the A_{1g} relaxation of the lattice. A set of such curves is shown in Fig. 1; they were calculated with $v_e = v_h = 0$ for absorption as discussed in Sec. III B. A set of five trial one-electron orbitals of the form given in Eq. (12) were used to form six two-electron configurations of the type given in Eq. (10b). Two compact orbitals of s-like (or a_{1g}) symmetry were used to describe the electron which is not primarily involved in the excitations to excited configurations. For those symmetries in which more than one state was calculated, e.g., $^1T_{1u,1}$ and $^1T_{1u,2}$, we chose two of the p-type (or t_{1u}) one-electron orbitals to minimize the first excited state and a third p orbital to describe the more diffuse higher state. Once again we emphasize that the exponential parameters in Eq. (12) are true nonlinear variational parameters, and that the integer exponents of r in that equation were subjected to limited variation. This, together with the linear variation coefficients in Eq. (9), gives quite flexible trial functions. No significant convergence problems were encountered except in the $^3T_{1u}$ state where the rapidly changing degree of localization of the wave function with lattice re-

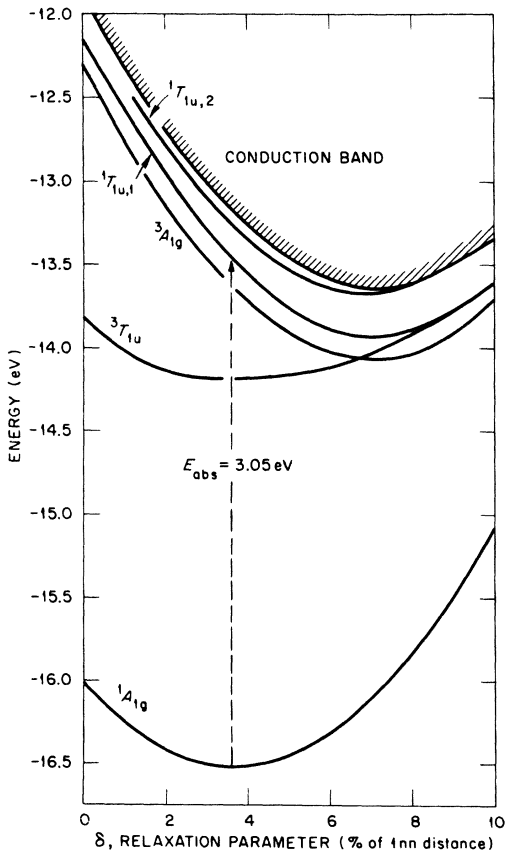

FIG. 1. A_{1g} configuration coordinate curves for F-center absorption.

laxation required additional care. We experimented with g- and f-type components in the a_{1g} and t_{1u} one-electron orbitals but found that they did not contribute significantly to the energy or wave functions. Excited-state orbitals of d-type (ϵ_g and t_{2g}) symmetry gave states lying just under the conduction band but we have not shown them since any role they may play in the physical processes of the defect is not yet apparent.

Figure 1 shows the bottom of the conduction band and a few words about its calculation are in order. First of all it should be kept in mind that ϵ_{HF} is adjusted within reasonable limits to give agreement with the ${}^1A_{1g} \rightarrow {}^1T_{1u,1}$ transition at ~3.1 eV. Within the context of the model, the true bottom of the conduction band E_{cond} including polarization-correlation effects introduced by polaron theory is calculated in much the same fashion as an F-center state. Thus by using Eqs. (18a) and (21a)–(21d) with $U_p = U_{cl}$, the expression for the electronic energy at the bottom of the band (no excitonic effects) is given by

$$E_{cond} = \epsilon(a_{1g}) + \epsilon_{HF} - (1 - k_\infty^{-1})\rho \ , \qquad (33a)$$

where $\epsilon(a_{1g})$ is the energy of the electron which remains well localized within the vacancy when the excited electron is removed to the bottom of the conduction band. It is calculated with sufficient accuracy by placing the excited electron in a very diffuse orbital. Of course, E_{cond} is not the same as the one-electron energy in a typical energy-band calculation because we include not only $\epsilon(a_{1g})$ but also the lattice-relaxation energy $\Delta E_{cr}(\delta)$.

The major contributions to the A_{1g} CC curve for the ${}^1T_{1u,1}$ electronic state are shown in Fig. 2. Although ΔE_p of Eq. (25) is not large compared to the other quantities, its variation is sufficient to effect the equilibrium position for the 1nn ions. Also, at the equilibrium position of the 1nn ions in emission, ΔE_p can change by approximately 1 eV when a transition occurs from the excited to the ground state.

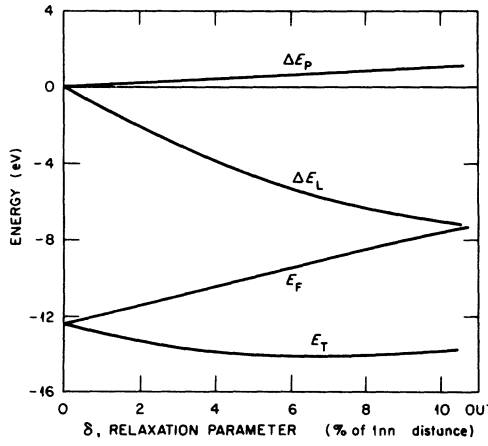

FIG. 2. Contributions from the quantities E_F, ΔE_L, and ΔE_P to the total energy E_T for the ${}^1T_{1u,1}$ absorption state of the F center in CaO, $\Delta E_L \equiv \Delta E_c + \Delta E_r$.

B. A_{1g} configuration coordinate curves—Emission

Most of the comments made above about the absorption curves apply equally to those for the emission process. However, in this case we must allow for the possibility that the electron in the excited state moves so slowly in a diffuse orbital that the ions are able to follow its motion to some extent; this is the classical ionic-polaron problem. In our model, $U_{ion}(r)$ of Eq. (17b) is introduced to take this effect into account. However, the value of v_h calculated from an equation such as that used to calculate v_e does not allow for enough energy of relaxation around the immobile hole (vacancy). This is clearly shown by comparison with the results of Mott-Littleton calculations for ionic relaxation around a negative-ion vacancy. As mentioned earlier, we do not yet have reliable quantitative information about the size of these ionic-polaron problems in the alkaline-earth oxides. In the absence of such information, Eq. (19b) is used here to give a rough estimate of v_e, and we take $v_h = v_e = v$. Thus, the bottom of the conduction band in emission is

$$E_{cond} = \epsilon(a_{1g}) + \epsilon_{HF} - (1 - \kappa_\infty^{-1})\rho - (\kappa_\infty^{-1} - \kappa_{st}^{-1})v \ . \qquad (33b)$$

Physically, the difference between Eqs. (33a) and (33b) means that during the absorption process the massive ions are unable to follow the motion of the electron and hole (vacancy) but that after the further lattice relaxation in the excited state they are. Figure 3 shows the CC curve diagram of Fig. 1 modified for the emission process.

C. Wave functions and charge densities

The two-electron wave function in the ground state is very well confined to the vacancy in both absorption and emission. This is illustrated in Fig. 4 where we have plotted the radial charge distribution given by

$$\rho(A_{1g}; r) = 2r^2 \int_0^\infty \int_{\Omega'} \int_{\Omega} |\Psi(\vec{r}, \vec{r}')|^2 r'^2 dr' \, d\Omega' \, d\Omega \ . \qquad (34)$$

The integration is over the solid angles of both electrons and the radial distribution of one of them; in the ground state both electrons have the same distribution from symmetry. In making this calculation, the orthogonality corrections to the

orbitals appearing in Eq. (11) were neglected. In the ground state, these terms make only small contributions in regions around the ions in the first few shells of neighbors. They would be important for the contact term of the hyperfine interaction if such existed for this center. The wave function used in obtaining the curve of Fig. 4 is for a 3.6% outward relaxation of the 1nn Ca^{2+} ions and corresponds to the minimum of the ground-state configuration-coordinate curve. The distribution changes very little in appearance with even larger relaxations and there is never any obvious tendency in the ground state for the charge to leak out of the vacancy.

The radial distribution function for the $^1T_{1u}$ state at 3.6% lattice distortion is shown in Fig. 5. The expression for the total charge distribution, given by Eq. (34), reduces to the sum of the a_{1g} and t_{1u} orbital probability distributions, i.e.,

$$\rho(T_{1u};r) = \rho(a_{1g};r) + \rho(t_{1u};r) \ . \qquad (35)$$

The calculation shows that the excited t_{1u} electron is well removed from the vacancy region while the a_{1g} orbital becomes even more localized than were

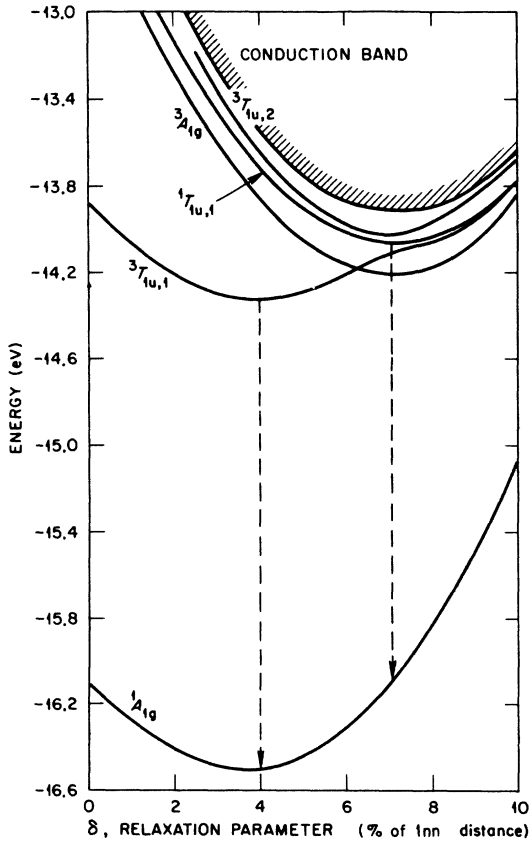

FIG. 3. A_{1g} configuration coordinate curves for F-center emission.

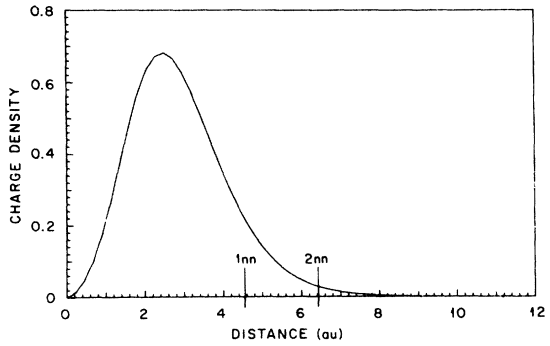

FIG. 4. CaO $^1A_{1g}$ radial charge density for a 3.6% A_{1g} outward lattice relaxation.

the a_{1g} orbitals in the ground state. The t_{1u} orbital occupies a region of space in which the effective-mass approximation is used in our model and therefore it is not surprising that it resembles a hydrogenic $2p$ orbital. It is interesting that the $^1T_{1u}$ excited-state charge density, like the $^1A_{1g}$ ground-state density, shows very little dependence on the A_{1g} relaxation of the 1nn ions. However, the reasons for this behavior are quite different in the two cases. In the ground state, the charge density always remains in the vacancy but in the $^1T_{1u}$ electron is so far outside of the vacancy that the movement of the 1nn ions has little effect on it. Table II illustrates the behavior of the integrated charge densities within the 2nn shell of ions as a function of the outward A_{1g} displacements of the 1nn Ca^{2+} ions.

The behavior of the $^1A_{1g}$ and $^1T_{1u}$ densities is in marked contrast to that of the $^3T_{1u}$ state, whose integrated 2nn charge depends strongly on the A_{1g} outward displacement of the 1nn ions. This is clearly shown in Table II. The 4% result corresponds to the minimum in the $^3T_{1u}$ configuration-coordinate curve. It suggests and the calculations show that in emission from the $^3T_{1u}$ state, the

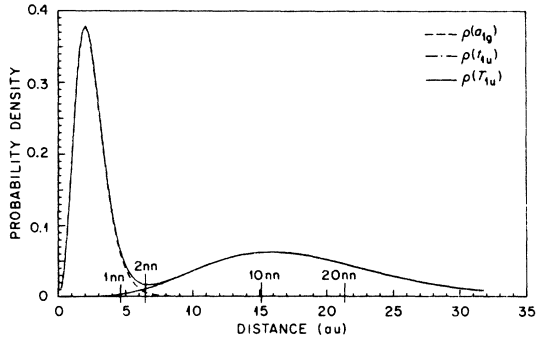

FIG. 5. CaO $^1T_{1u}$ radial charge density for a 3.6% A_{1g} outward lattice relaxation. $\rho(a_{1g})$ and $\rho(t_{1u})$ are the densities of the a_{1g} and t_{1u} electrons, respectively, and $\rho(T_{1u})$ is their sum.

electron in the t_{1u} orbital has a considerable overlap with the orbitals on the 1nn Ca^{2+} ions and as a consequence it is quite sensitive to both cubic and noncubic distortions of these ions. The 8% result illustrates the fact that as the 1nn ions relax outward and the Madelung well is thus raised, the t_{1u} charge rapidly leaks out into the crystal. The $^3T_{1u}$ densities for 4% and 8% relaxation are shown in Figs. 6 and 7, respectively.

D. Electron-phonon interaction

The model we have used in the calculations described herein allows us to compute the electron-lattice interaction for A_{1g}, E_g, and T_{2g} lattice vibrations. The calculations for the A_{1g} modes in different electronic states are straightforward since the effective force constants can be extracted directly from the various CC curves shown in Figs. 1 and 3. The corresponding curves for E_g modes are not much more difficult to compute since they merely involve finding the electronic energy of the various states when the $1nn$ ions are displaced in one of the two degenerate E_g configurations. The T_{2g} modes are considerably more difficult to cope with because T_{2g} lattice distortions mix T_{1u} electronic states. In the interest of keeping the present paper within a reasonable length, we will not give the details of such a calculation here.

The so-called Huang-Rhys factor can be deduced from a set of CC curves. It has strict meaning only in linear-coupling theory in the absence of dynamic Jahn-Teller coupling; for our purposes this implies that the force constants in the ground and excited electronic states are the same. This is not exactly the case in the present calculations, but it is probably a sufficient approximation in light of the accuracy of the available experimental data. If we let K_a be the force constant in the ground and excited states in absorption and X_a be the CC separation of the two minima, then the Huang-Rhys factor for absorption is given by

$$S_a = \tfrac{1}{2} K_a X_a^2 / h\nu_a. \tag{36}$$

The effective frequency ν_a can be calculated if a mass associated with the oscillator is assumed. Frequently this mass is taken to be that of the $1nn$ ions but this will hardly ever be a valid assumption since the displacement of these ions alone will seldom form true vibrational eigenvectors. Nevertheless, it does give some idea of whether or not ν_a will fall near a peak in the symmetry-projected density of states of the perfect crystal. We have used this approximation here, and find the following values for the relevant parameters in absorption: $S_a \simeq 10$, $K_a = 1.9 \times 10^6$ dyn cm^{-1}, $X_a = 0.036 a_0$, and $\nu_a = 365$ cm^{-1}. The halfwidth of the absorption band in linear-coupling theory can be related to these quantities by the equation

$$H_a = (8 \ln 2)^{1/2} h\nu_a (S_a)^{1/2}. \tag{37}$$

From this we calculate a halfwidth of 0.33 eV which should be compared to an experimental[28] value of roughly 0.50 eV. As our CC curves indicate, a second $^1T_{1u}$ electronic state lies just above the lowest $^1T_{1u}$ state. Transitions to both of these two states give a combined band with a halfwidth of

TABLE II. Integrated charge within the second-nearest-neighbor shell of ions in CaO as a function of the A_{1g} outward distortion of the first-nearest-neighbor ions for the lowest energy state of each symmetry.

δ [a]	$^1A_{1g}$	$^3A_{1g}$	$^1T_{1u}$	$^3T_{1u}$
0	1.98	1.05	1.04	1.93
2	1.98	1.02	1.01	1.88
4	1.97	1.01	1.01	1.72
6	1.96	1.01	1.00	1.52
8	1.93	1.00	1.00	1.05
10	1.89	1.00	1.00	1.01

[a] δ measures the outward distortion of the 1nn ions in % of the perfect lattice anion-cation distance.

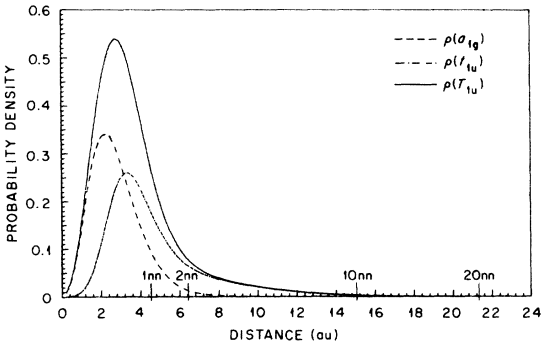

FIG. 6. CaO $^3T_{1u}$ radial charge density for a 4% A_{1g} outward relaxation. Notation follows that of Fig. 5.

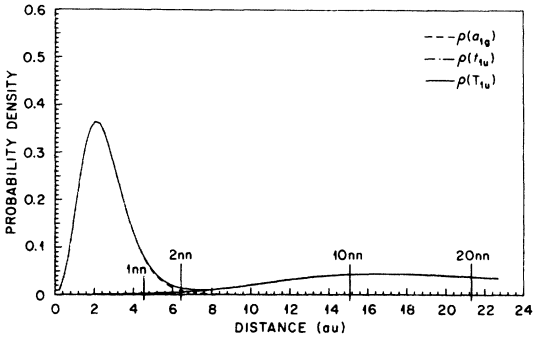

FIG. 7. CaO $^3T_{1u}$ radial charge density for an 8% A_{1g} outward relaxation. Notation follows that of Fig. 5.

0.5 eV. The suggestion is that the F band is a composite and indeed this appears to be likely from the experimental shape.

Both experiment and theory show that the emission process is considerably more complicated than the absorption. For the lowest T_{1u} electronic state, the shape of the emission CC curve is altered from the absorption curve due to ionic polarization effects and the attendant additional delocalization of the wave function. For emission from the $^1T_{1u}$ state, we find $K_{e1}(A_{1g}) = 2.2 \times 10^6$ dyn/cm and $\nu_{e1}(A_{1g}) = 390$ cm^{-1}. Under the assumptions of our calculation, this gives a Huang-Rhys factor of approximately 10. For the $^3T_{1u}$ state, we calculate the minimum to be at 4% outward relaxation of the 1nn ions which is only slightly greater than X_a. Its coupling to the A_{1g} modes gives $K_{e2}(A_{1g}) = 1.6 \times 10^6$ dyn cm^{-1} and $\nu_{e2}(A_{1g}) = 331$ cm^{-1}. Assuming linear coupling, the A_{1g} Huang-Rhys factor is 0.13.

Calculations for E_g and T_{2g} vibrations were carried out for the $^3T_{1u}$ and $^1T_{1u}$ states in emission. At an outward A_{1g} relaxation of 4%, the minimum energy when the system is in the $^3T_{1u,z}$ state occurs for an $E_g\epsilon$ distortion [$Q_1(E_g\epsilon)$ of Table I] in which the ions along the z axis displace outward by an additional 1.4% and the ions along the x and y axes inward by one-half that amount. (A corresponding $E_g\theta$ distortion also occurs, of course.) A similar but much more-complex calculation was made for the T_{2g} distortion $Q_1(T_{2g})$. As already mentioned, unlike E_g and A_{1g} modes, the T_{2g} modes mix the electronic T_{1u} states. Our results for emission from the $^3T_{1u}$ state are summarized in Table III. We found little or no Jahn-Teller coupling in the $^1T_{1u}$ state due to its diffuse nature. No coupling is expected in the $^1A_{1g}$ and $^3A_{1g}$ states for symmetry reasons and, as a check on our programs, we verified that there was none by direct calculation.

V. DISCUSSION

Our calculated results for the F-center absorption agree reasonably well with the experimental data available. This was expected for the absorption band maximum since the calculated and measured positions were forced to coincide approximately by our choice of ϵ_{HF}. The measured peak is at 3.1 eV at 78 °K, and we fitted our calculated peak to approximately 3.05 eV using mostly room-temperature data. The absorption halfwidth is of more interest, but the overlap of the F and F^+ bands make it difficult to determine this experimentally. An experimental halfwidth of ~0.5 eV was estimated from the absorption band measurements of Modine.[28] This number and an approximate band shape were obtained by attempting to subtract the small contribution of the F^+ band. This procedure gave a very asymetrical band with a long almost-flat tail on the high-energy side. From the CC curves of Fig. 1 this tail would appear to arise from transitions to states lying just below and even within the conduction band. In absorption, the bottom of the conduction band lies about 0.3 eV above the first $^1T_{1u}$ state and transitions to it would fall well within the high-energy tail of the experimental band. In spite of the rather peculiar band shape, we calculated a halfwidth using standard equations from linear coupling theory. We obtained the value of 0.33 eV, mentioned in Sec. IV for the transition from the $^1A_{1g}$ to the first $^1T_{1u}$ excited state. The second $^1T_{1u}$ level, lying roughly 0.2 eV above the first and having about the same halfwidth, was found to contribute almost equally to the strength and halfwidth. The relative contributions of the two states depend on their relative oscillator strengths. The oscillator strength for each of the two transitions was obtained from the expression

$$f(^1A_{1g} \rightarrow {}^1T_{1u}) = \tfrac{2}{3}\Delta E \left| \langle {}^1A_{1g} \left| \vec{r}_1 + \vec{r}_2 \right| {}^1T_{1u} \rangle \right|^2, \qquad (38)$$

in which ΔE is the appropriate transition energy. A significant simplification is achieved in the calculation of the dipole matrix elements by ignoring the contributions that arise from the orthogonalization of the vacancy centered functions to the core states on the neighboring ions. This approximation was apparently adequate for the F center in the alkali halides.[4] Using this approximation here, however, we obtained $f(^1A_{1g} \rightarrow {}^1T_{1u,2}) = 0.08$. An examination of Figs. 4 and 5 and Table III, which contain information about the charge density in the various states, suggests why we calculate such small oscillator strengths. The charge density in the $^1A_{1g}$ state is localized in the vacancy whereas in the $^1T_{1u,1}$ and higher states it is well outside of the vacancy. Thus, the matrix elements of $\vec{r}_1$ and $\vec{r}_2$ appearing in Eq. (38) might be expected to be small and the calculations show this indeed to be the case. As far as we can ascertain, an experimental value for the oscillator strength in CaO has never been reported, undoubtedly due in large part to the aforementioned difficulties with the line shape. Nevertheless, our values appear to be too

TABLE III. Summary of results for the $^3T_{1u}$ emission state of CaO.

Mode	S	E_{JT} (eV)	$h\nu$ (cm^{-1})
A_{1g}	0.13	•••	331.3
E_g	2.14	−0.071	265.5
T_{2g}	0.76	−0.027	285.6

small. We believe this to be due to the neglect of the Ca^{2+} and O^{2-} core contributions, and to the change in electronic polarization of these ions during the transition from one state to another. Although compatibility with the rough experimental data on the halfwidth can be obtained, neither the experimental nor the theoretical results on the band shape are in a completely satisfactory state. In any case, the value of the Huang-Rhys factor is well outside the range for which vibronic structure might be observed, and none has been observed on the absorption band.

As mentioned in Sec. II, the CC curves shown in Fig. 3 have already proved useful in elucidating certain aspects of the emission spectra of the F center in CaO. For some time it was felt that the $^1T_{1u} \rightarrow {}^1A_{1g}$ emission occurred at 2.5 eV, with the $^3T_{1u} \rightarrow {}^1A_{1g}$ occurring at 2.0 eV (Ref. 13); at least one theoretical calculation[19] lent support to this interpretation. However, all of our attempts to adjust the parameters in our model to yield these emission lines, while at the same time keeping the absorption at about 3.1 eV, failed. In all of these calculations, the model consistently predicted that the $^3T_{1u} \rightarrow {}^1A_{1g}$ and $^1T_{1u} \rightarrow {}^1A_{1g}$ transitions should lie within about 0.1 eV of one another. We obtain similar results for the corresponding transitions in MgO, where only one emission line has been identified with the F center. These results led to the recent reexamination of the emission spectra of the F center in CaO by Bates and Wood,[14] who have shown that the 2.5-eV band is not related to a transition of the F center. Measurements[15] of luminescence spectra from 50 → 350 °C further confirmed the predictions of the model. They indicate that at low temperatures (below 25 °C), it is the $^3T_{1u}$ level that is predominantly populated, and therefore the $^3T_{1u} \rightarrow {}^1A_{1g}$ band is dominant. As the temperature is increased, the $^1T_{1u}$ level becomes populated at the expense of the $^3T_{1u}$ level, and above 300 °C, the $^1T_{1u} \rightarrow {}^1A_{1g}$ band contributes strongly to the luminescence. In fact, a two-peaked structure is observed. Theoretical calculations[15] based on emission curves quite similar to those shown in Fig. 3 confirm this interpretation. An earlier study[29] of the temperature dependence of the $^3T_{1u} \rightarrow {}^1A_{1g}$ emission band for $T = 5$–300 °K showed that for temperatures less than 90 °K, the band is reasonably Gaussian, but that it becomes rather asymmetric above this temperature. These results are consistent with the temperature-dependent growth of the $^1T_{1u}$ contribution to this band.

Our calculations of the strength of the coupling of the $^3T_{1u}$ electronic state to the A_{1g}, E_g, and T_{2g} vibrational modes now support the interpretation given by Edel *et al.*[16,17] of the results of their optical spin-resonance measurements. They concluded that the Jahn-Teller coupling of this state to the E_g modes is strong and that the coupling to the A_{1g} and T_{2g} modes is weak. In our earlier calculations, we found the A_{1g} and E_g coupling to be approximately equal and we had not calculated the T_{2g} coupling. Subsequently, we found that a relatively minor change in the value of ϵ_{HF} [Eq. (21c)] would give the present results which are in rather good agreement with the experimental conclusions. However, we point out again that portions of the analysis of Edel *et al.* appear to be based on an overly simplified model. Apparently they have assumed that the Jahn-Teller splittings and the spin-orbit coupling parameters in the $^3T_{1u}$ and $^1T_{1u}$ states are the same. Our calculations clearly show that this cannot be the case because of the different degrees of localization of the wave functions of the two states. Thus, the spin-orbit parameter and level splitting involved in the determination of the oscillator strength for the $^3T_{1u} \rightarrow {}^1A_{1g}$ emission are generally not the same as the corresponding quantities involved in determining the g factors of the $^3T_{1u}$ state.

The results shown in Figs. 1 and 3 indicate that it may be possible to study the energy level scheme of the F center in the alkaline-earth oxides further by excited-state spectroscopy. The lowest $^3T_{1u}$ state in CaO has a lifetime of milliseconds and a $^3A_{1g}$ state apparently lies a few tenths of an eV above it. Optical pumping into the $^3T_{1u}$ state may allow the $^3T_{1u} \rightarrow {}^3A_{1g}$ transition to be detected.

ACKNOWLEDGMENTS

We would like to thank Mark Mostoller for help with certain aspects of the calculations, and J. B. Bates, F. A. Modine, M. M. Abraham, and Y. Chen for several useful discussions.

† Research sponsored by the U. S. ERDA under Contract with Union Carbide Corp.

[1]Some preliminary results on the F center in CaO have been reported; R. F. Wood and T. M. Wilson, Solid State Commun. 16, 545 (1975).
[2]R. F. Wood and H. W. Joy, Phys. Rev. 136, A451 (1964).
[3]U. Öpik and R. F. Wood, Phys. Rev. 179, 772 (1969).
[4]R. F. Wood and U. Öpik, Phys. Rev. 179, 783 (1969).
[5]R. F. Wood and U. Öpik, Phys. Rev. 162, 736 (1967).
[6]R. F. Wood and R. L. Gilbert, Phys. Rev. 162, 746 (1967).
[7]A. Meyer and R. F. Wood, Phys. Rev. 133, A1436

(1964).
[8]R. F. Wood, Phys. Rev. 151, 692 (1966).
[9]B. Henderson and J. E. Wertz, Adv. Phys. 17, 749 (1968).
[10]A. E. Hughes and B. Henderson, in *Point Defects in Crystals*, edited by J. H. Crawford, Jr. and L. M. Slifkin (Plenum, New York, 1972).
[11]L. A. Kappers, R. L. Kroes, and E. B. Hensley, Phys. Rev. B 1, 4151 (1970).
[12]W. C. Ward and E. B. Hensley, Phys. Rev. 175, 1230 (1968).
[13]B. Henderson, S. E. Stokowski, and T. C. Ensign, Phys. Rev. 183, 826 (1969).
[14]J. B. Bates and R. F. Wood, Phys. Lett. A 49, 389 (1974).
[15]J. B. Bates and R. F. Wood, Solid State Commun. 17, 201 (1975).
[16]P. Edel, C. Hennies, Y. Merle D'Aubigné, R. Romestain, and Y. Twarawski, Phys. Rev. Lett. 28, 1268 (1972).
[17]P. Edel, Y. Merle D'Aubigné, and R. Louat, J. Phys. Chem. Solids 35, 67 (1974).
[18]V. I. Neeley and J. C. Kemp, Bull. Am. Phys. Soc. 8, 464 (1963).
[19]H. S. Bennett, Phys. Rev. B 1, 1702 (1970).
[20]J. C. Slater, Phys. Rev. 81, 385 (1951).
[21]See, for example, A. B. Kunz, Phys. Rev. B 8, 1690 (1973).
[22]Y. Toyozawa, Prog. Theor. Phys. 12, 422 (1954).
[23]H. Haken and W. Schottky, Z. Phys. Chem. (Frankfort) 16, 218 (1958).
[24]N. F. Mott and M. J. Littleton, Trans. Faraday Soc. 34, 485 (1938).
[25]M. Mostoller and R. F. Wood, Phys. Rev. B 7, 3953 (1973).
[26]I. M. Boswarva and A. B. Lidiard, Atomic Energy Research Establishment Report No. T.P. 232 (revised), Harwell, England (unpublished); and Philos. Mag. 16, 805 (1967).
[27]J. P. Dahl and C. J. Ballhausen, in *Advances in Quantum Chemistry*, edited by P. O. Löwdin (Academic, New York, 1968), Vol. 4, p. 170.
[28]F. A. Modine, Phys. Rev. B 7, 1574 (1973).
[29]B. Henderson, Y. Chen, and W. A. Sibley, Phys. Rev. B 6, 4060 (1972).